

**REVERSIBLE CHANGES INDUCED BY TEMPERATURE IN
THE SPHERULITIC BIREFRINGENCE OF NYLON 6 9**

**Sara K. Murase¹, María Teresa Casas¹, Juan Carlos
Martinez³, Francesc Estrany^{1,2}, Lourdes Franco^{1,2*}, Jordi
Puiggali^{1,2,*}**

¹Departament d'Enginyeria Química, Universitat Politècnica de Catalunya, Av. Diagonal 647, Barcelona E-08028, SPAIN

²Center for Research in Nano-Engineering, Universitat Politècnica de Catalunya, Campus Sud, Edifici C', C/Pasqual i Vila s/n, Barcelona E-08028, SPAIN

³ALBA Synchrotron Light Facility, Ctra. BP 1413 km. 3,3 | 08290 | Cerdanyola del Vallès| Barcelona | SPAIN (www.albasynchrotron.es)

Correspondence to: Jordi Puiggali (E-mail: Jordi.Puiggali@upc.edu)

ABSTRACT

Spherulitic morphologies of nylon 6 9 as an example of an even-odd nylon were studied by optical microscopy. A well-defined dependence on crystallization temperature was found. In particular, positively birefringent spherulites were characteristic for temperatures higher than 232 °C, low birefringence spherulites developed between 232 and 225 °C, positive ringed spherulites were found between 225 and 220 °C, and finally negative fibrillar spherulites were formed at temperatures lower than 220 °C. These optical properties were clearly different from those observed with even-even nylons (e.g., negative and positive birefringence for high and low temperatures, respectively), and may derive from the peculiar crystalline structures determined for even-odd nylons. Furthermore, low birefringence spherulites were characterized by a flat-on lamellar disposition and reversibility of the birefringence sign in the 80-120 °C temperature interval (positive and negative values at high and low temperatures, respectively).

Real time WAXD profiles taken during heating and cooling processes demonstrated that different crystalline structures (named I, II and III) developed depending on the temperature and crystallization procedure of samples (e.g., from solution or from the melt state). Crystalline structures were characterized by the formation of hydrogen bonds along two crystalline directions in all cases, a peculiar arrangement that may account for the development of positive and negative spherulites in a more simple way than formulated for conventional polyamides having a single hydrogen bonding direction. DSC and FTIR data also showed a complex structural behavior with structural transitions in the 80-120 °C range, a region that corresponds to birefringence sign reversibility.

Keywords: Even-odd nylons, spherulites, birefringence, Brill transition, hydrogen bonds, infrared spectra, differential scanning calorimetry.

INTRODUCTION

Despite the tremendous importance of polyamides in society and enormous effort devoted to research and development of nylons, publications on the structure of non conventional nylons (i.e., those different from even and even-even series) are scarce. However, odd derivatives are gaining interest due to the development of materials based on renewable resources because of concerns over long-term availability of chemicals derived from fossil resources [1,2]. Nylons 5 6 [3-6], 6 9 [7] and 13 6 [8] can be considered in this context. Furthermore, the ferroelectric behavior of odd numbered polyamides has been discovered, with remanent polarization being linearly dependent upon the dipolar density of amide groups [9,10]. Specifically, nylon 6 9 has also been considered as a material with piezoelectric activity due to its peculiar structure [7].

The crystalline structure of conventional even-even nylons is defined by a stack of hydrogen bonded sheets that progressively (α -form) or alternatively (β -form) arranged themselves parallel to the plane of the sheet [11,12]. Fiber diffraction patterns of such structures are characterized by strong equatorial reflections at spacings close to 0.43 and 0.38 nm. Linear hydrogen bonds between molecules confined in the sheets could be formed for an all-trans conformation, giving rise to strong interactions and a minimum packing energy. A pseudohexagonal arrangement defined by strong equatorial spacings very close to 0.415 nm and named γ -form has been determined for several odd-odd nylons (e.g., nylon 7 7) [13]. In this case, amide groups are rotated from the plane defined by the methylene carbons in such a way that linear hydrogen bonds are established along a single direction between molecules of neighbouring sheets.

More complex geometries have been postulated for the room temperature structures of polyamides containing glycine units [14] and also of several odd-even and even-odd

nylons [8,15-26]. These structures were characterized by the establishment of hydrogen bonds along three and two directions as a consequence of the conformational preferences of glycine residues and the inability to establish a saturated intrasheet hydrogen bonding scheme when an all-trans molecular conformation was assumed and odd diamine or diacid units were involved (Figure 1a).

The rotation of the two amide groups of the odd unit in opposite directions to the plane defined by the methylene carbon atoms allowed the formation of linear hydrogen bonds along two directions when neighboring chains were conveniently sheared parallel to the chain axis (Figure 1b). This structure was consistent with the typical diffraction spacings of α - and β -forms and was defined by a centered monoclinic unit cell, with the chain axis projection corresponding to a rectangular unit cell whose diagonals matched the two hydrogen bonding directions. This peculiar structure has also been recently postulated for even polyoxamides with methyl side-groups (i.e., poly(2-methyl-1,8-octamethyleneoxamide) [27].

It is worth mentioning that the structure of conventional nylons has usually a continuous evolution with temperature towards a pseudo-hexagonal packing that is achieved at the so-called Brill transition temperature [28-34]. Unfortunately, low resolution or ambiguous X-ray diffraction data do not provide a good understanding of this transition. Recent works based on FTIR data suggest that high temperature pseudo-hexagonal arrangements are a result of the conformational disorder of polymethylene segments rather than of disruption of hydrogen bonds [35-37].

Morphology and optical properties of melt crystallized spherulites of polyamides also show some puzzling features. Thus, even-even nylons (e.g., nylon 6 6) render negative spherulites at crystallization temperatures near their melting point and positive spherulites at lower temperatures [12,38]. The change in optical properties of these

nylons was explained by the stacking of their constitutive hydrogen bonded sheets. Specifically, linear hydrogen bonds were oriented along the spherulite radial (positive birefringence) and tangential (negative birefringence) directions. Nevertheless, the reason why the growth mechanism varied so drastically (radial or tangential direction of hydrogen bonds or sheets) at a given temperature remains unclear.

Properties of spherulites of even-odd nylons have been less studied, but pioneering and phenomenological works of Magill [39] performed with nylons 4 9, 6 7 and 6 9, and more recently results reported for nylon 4 7 indicate a peculiar behavior [19]. Thus, a reversible change in birefringence induced by temperature was detected. This feature is highly interesting since cannot be explained by a simple change in the sheet arrangement inside the spherulite as was postulated for structures having a single hydrogen bonding direction. It should be emphasized that birefringence of spherulites is still a hot topic [40-42], especially when different lamellar orientations (e.g., edge-on and flat-on) are considered. To the best of our knowledge, no explanations for reversible changes in birefringence of nylons induced by temperature have been reported. In some binary systems (e.g., poly(hydroxyl butyrate)/poly(methyl acrylate blend), reversibility of birefringence was accounted for by a crystallization-induced phase separation [43].

The present work is focused on nylon 6 9 due to its peculiar structure based on two hydrogen bonding directions. The main objective is the study of thermally induced structural transitions and their influence on optical properties of spherulites. New data can help the understanding of the complex behavior of polyamides that arises from the relevance of the hydrogen bonding intermolecular interactions.

EXPERIMENTAL SECTION

Materials

Nylon 69 was synthesized by interfacial polycondensation of 1,6-diaminohexane and azeloyl chloride using toluene as organic solvent and sodium hydroxide as proton acceptor and following the procedure previously described for similar nylons [16]. The polymer was purified by precipitation with water of a formic acid solution. Nylon 69 was obtained with a yield of 65%. Number average molecular weight and polydispersity index were 25,000 g/mol and 2.2, respectively, as determined by GPC and using poly(methyl methacrylate) standards.

Measurements

Time resolved WAXD experiments were carried out at the NCD beamline (BL11) of the Alba synchrotron radiation light facility of Cerdanyola del Vallès (Catalunya). The beam was monochromatized to a wavelength of 0.100 nm. Polymer samples were confined between Kapton films and then held in a Linkam hot stage with temperature control within ± 0.1 °C. WAXD profiles were acquired during heating and cooling runs in time frames of 20 s and a rate of 3 °C/min. The WAXD detector was calibrated with diffractions of a standard of a Cr₂O₃ sample. The diffraction profiles were normalized to the beam intensity and corrected considering the empty sample background. Deconvolution of WAXD peaks was performed with the PeakFit v4 program by Jandel Scientific Software using a mathematical function known as “Gaussian area”.

IR absorption spectra were recorded on a Jasco FT/IR 4100 Fourier transform spectrometer in the 4000–600 cm⁻¹ range. A Specac MKII Golden Gate Single Reflection Diamond ATR system, which can be used up to 200 °C, and a high stability 4000 series controller were also employed.

Calorimetric data were obtained by differential scanning calorimetry with a TA Instruments Q100 series equipped with a refrigeration cooling system. Experiments were conducted under a flow of dry nitrogen with a sample weight of approximately 5 mg and calibration was performed with indium.

Basic thermal characterization was obtained from cooling runs (10 °C/min) of melted samples and heating runs (20 °C/min) of as-synthesized, melt crystallized and quenched samples.

Spherulitic morphologies were analyzed by optical microscopy using a Zeiss Axioskop 40 Pol light polarizing microscope equipped with a Linkam temperature control system configured by a THMS 600 heating and freezing stage connected to an LNP 94/2 liquid nitrogen cooling system. A first-order red tint plate was employed to determine the birefringence sign under crossed polarizers. Micrographs were taken with a Zeiss AxioCam MRc5 digital camera. Spherulites were grown from homogeneous thin films prepared by melt pressing. Small sections of these films were pressed or smeared between two cover slides, inserted in the hot stage, melted at approximately 10 °C above their melting point for 5 minutes to wipe out sample history effects and quickly cooled to the selected crystallization temperature.

For AFM studies, thin films placed on cover slides were melt crystallized at the selected temperatures. Height and amplitude images of spherulites were obtained with a Molecular Imaging PicoSPM using a NanoScope IV controller in ambient conditions and a scan window size of 10 x 10 μm^2 . The tapping mode AFM was operated at constant deflections (i.e., vertical constant force with gold-coated silicon nitride). Row scanning frequency was set to 1 Hz and physical tip-sample motion speed was 10 $\mu\text{m/s}$.

RESULTS AND DISCUSSION

Time resolved WAXD data on heating and cooling processes: Brill transition

Single crystal electron diffraction and X-ray fiber diffraction data indicated that at room temperature nylon 6 9 crystallized according to the above structure with two hydrogen bonding directions and a *C*-face centered monoclinic unit cell with parameters $a = 0.793$ nm, $b = 0.524$ nm, c (chain axis) = 4.04 nm and $\beta = 108^\circ$ [20]. At high temperature a hexagonal unit cell was also reported; a single equatorial reflection was observed at 0.420 nm in the fiber diffraction patterns. It was postulated that the alkane segments existed in a mobile phase and equivalent hydrogen bonds populated the three principal (hexagonal) directions [20]. Fiber patterns of melt quenched samples were characterized by strong equatorial reflections at 0.420 and 0.415 nm (as observed in a typical γ -form) but in this case a two-chain orthorhombic unit cell with parameters $a = 0.830$ nm, $b = 0.487$ nm and $c = 4.00$ nm was postulated. It was assumed that interchain hydrogen bonds were formed in all three principal crystallographic directions, as observed in the high temperature structure. However, bonds formed along the two unit cell diagonals were equivalent and stronger [20].

Figure 2a shows the evolution of X-ray diffraction profiles of the as-synthesized sample during heating at a rate of 3 °C/min. A continuous evolution of the typical reflections at 0.435 and 0.376 nm (form I) was observed. The respective peaks became progressively closer until a majority peak (ca. 0.423 nm) indicative of a typical pseudo-hexagonal arrangement (hereafter named form III) was detected at a temperature of 235 °C as a result of the Brill transition. It should be noted that no transition towards another crystalline structure (hereafter named form II) was observed during the intermediate steps of the heating process. This feature is in contrast with previous diffraction profiles of nylon 4 7 (inset of Figure 2a) where a form I to form II transition is described

between 60 and 120 °C [19]. In this case, the intensity of the two equatorial reflections at 0.430 and 0.389 nm gradually diminished during heating while new reflections with increasing intensity appeared near 0.422 and 0.407 nm.

Figure 2b shows the X-ray diffraction profiles recorded during the cooling process (3 °C/min) from the melt state. In this case, the evolution is more complex and reveals three significant features.

a) A narrow intense peak appeared around 0.423 nm during crystallization, which should be associated with form III (i.e., that achieved after the Brill transition temperature during the heating process). Profiles also showed some low intensity peaks at 0.429 and 0.418 nm that indicated that form III did not have a truly pseudo-hexagonal arrangement (probably because two hydrogen bonding directions persist in the high temperature structure). During the cooling process the 0.429 nm peak moved to lower spacings and merged into the predominant peak at a temperature close to 180 °C while the peak at 0.418 nm also moved slightly to lower spacings and decreased in intensity since it could hardly be detected at room temperature (blue arrows). In conclusion, form III experienced a slight change in cell dimension on cooling that may simply be due to a typical contraction caused by the temperature decrease. In any case, the deviation from a pseudo-hexagonal arrangement clearly increased at lower temperatures. Therefore, the three planar directions that define a hexagonal packing were not equivalent, and probably a model based on a random distribution of hydrogen bonds along these three equivalent directions could be discarded.

b) The reflection at 0.418 nm seemed to split at around 110 °C, giving rise to a new reflection at 0.411 nm that moved to 0.404 nm (red arrow) and increased in intensity during the cooling process. Hence, profiles showed a transformation from form III to a new one named form II. The reflection at 0.423 nm did not seem affected during the

cooling process since it can be assumed as a common spacing for both forms III and II (i.e., it moved to 0.421 nm in the room temperature pattern). The polymorphic transition also seems supported by the different intensity ratio between reflections at 0.423 and 0.418 nm (form III) and those appearing at 0.421 and 0.404 nm (form II). In the first case, the ratio was high whereas in the second case intensities were highly similar.

c) Two new reflections appeared at temperatures below 90° C and increased in intensity at lower temperatures while evolving in a divergent way (see green arrows) towards the characteristic spacings (0.436 and 0.375 nm) of form I. It is clear that reflections were not detected at higher temperatures and that they were not a consequence of the typical Brill transition observed during cooling. Specifically, the main reflection, which is associated with the pseudohexagonal packing, did not split into the two reflections, which progressively deviated towards higher (0.436 nm) and lower (0.375 nm) spacings usually shown in Brill transitions during cooling processes. In summary, a morphological transition seemed to occur at temperatures lower than 90 °C, giving rise to the appearance of a minor ratio of form I (from form III or even from the also appearing form II).

The variation in intensity of the strongest peak (0.423-0.421 nm) was useful to monitor the different processes that occur in the cooling step, as shown in Figure 3a. This peak appeared and increased in intensity within the temperature range of 240-170 °C, where primary crystallization into form III took place, and then (i.e., between 170 and 150 °C) increased slightly due to secondary crystallization. Intensity remained practically constant in the 150 °C and 110 °C interval. A significant decrease was subsequently detected at lower temperatures because of the development of forms I and II.

It is important to note that the X-ray profile obtained at room temperature corresponded to a mixture of structures, as can be deduced from the deconvoluted profile in Figure 3b,

which contrasts with the one obtained from the as-synthesized sample. In addition, the structural change observed on heating was not reversible on cooling.

For the sake of completeness, Figure 4a shows representative X-ray diffraction profiles taken during heating and cooling runs at room temperature with the as-synthesized sample before starting the heating process and at the end of the cooling process. Profiles of similar structures (form III) obtained on heating just before melting (235 °C) and on cooling at the end of crystallization (220 °C) and those obtained at intermediate stages of 165 and 150 °C (form I on heating and form III on cooling) are also shown. Representative diffraction patterns taken during the heating process are given in Figure 4b to clarify the absence of reflections associated with form II.

In summary, nylon 6 9 has different crystalline structures depending on the crystallization procedure (e.g., from solution or from melt) and temperature. However, all structures seem constituted by molecular arrangements where hydrogen bonds are formed along two directions.

DSC data on thermally induced transitions

Thermal behavior of nylon 6 9 is highly complex, as deduced from the four scan protocol in Figure 5, where multiple exothermic and endothermic processes can be seen. The following observations can be made:

- a) Multiple melting peaks (ordered by increasing temperature from I to IV) can be observed for the as-synthesized sample. They appear as a consequence of lamellar reordering processes (II and IV) and even from different polymorphic forms (I and III for peaks I to II and III to IV, respectively).
- b) Crystallization from the melt rendered a well-defined peak around 207 °C (for a cooling rate of 20 °C/min) but also a broad exotherm that extended up to 100 °C. This is

indicative of a secondary crystallization because it occurs at a higher temperature interval than the structural changes detected in WAXD experiments.

c) Peaks resulting from reordering of lamellae (II and IV) were practically not observed by DSC when samples crystallized from melt. Thus, thinner lamellae (those associated with peaks I and III) were more stable after slow crystallization, finally hindering the reordering process.

d) Intensity of peak I was higher for the melt quenched sample than for the melt crystallized one, in agreement with FTIR observations, which indicated a greater content of form I in the quenched sample, as will be explained.

e) A broad exothermic peak (70-140 °C) and a well-defined exothermic peak at 204 °C could be detected in the heating run of the melt quenched sample (and even of the melt crystallized sample). They corresponded to the polymorphic transition from forms I or II to form III and hot crystallization into form III of melted form I crystals. The first point is in agreement with the solid state transition detected from WAXD data while the second will be discussed below.

Lamellar reordering processes are evidenced by DSC traces obtained at different heating rates (Figure 6). Thus, the intensity of peak IV decreased with respect to peak III when the heating rate was increased since molecular chains had insufficient time to be reordered and gave rise to thicker lamellae with a higher melting point. We also interpret that peak II corresponds to the thickening of crystals having the form I structure. Note also that this process cannot occur at the highest heating rate (i.e., 50 °C/min). In this case, the absence of the endothermic peak II, which is associated with fusion of thicker lamellae, highlights a previous exothermic event that necessarily implies the formation of form III crystals from previously melted form I crystals.

Figure 7 shows DSC traces of samples isothermally crystallized at temperatures higher than 215 °C and subsequently cooled to room temperature. Only peaks III and IV were detected at crystallization temperatures lower than 225 °C as a complete crystallization was achieved in this case. The temperature corresponding to peak III increased slightly with crystallization temperature, revealing the formation of thicker lamellae. In fact, a typical linear Hoffman-Weeks plot [44] could be obtained considering the relation of the peak III melting temperature with the crystallization temperature (Figure 8). An equilibrium melting temperature of 238.7 °C was deduced. Logically, the temperature of peak IV was independent of the crystallization temperature since it corresponded to the fusion of thicker crystals resulting from lamellar reordering during the heating process. DSC traces also showed that the thickening process was hindered when more perfect crystals were obtained; that is, when the crystallization temperature was increased. Note also that a clear exotherm was detected for samples crystallized at the lowest temperatures due to an enhanced reordering process.

DSC traces of samples crystallized at temperatures equal or higher than 225 °C are highly interesting because only a small ratio developed at this temperature, and consequently main crystallization took place during the subsequent cooling process. Therefore, traces showed the appearance of an additional endothermic peak (227 °C - 230 °C) associated with the melting process of thick crystals having the form I structure. These crystals underwent a polymorphic transition during heating, giving rise to thick form III crystals (peak IV), as can be clearly seen in the trace of the sample crystallized at 232 °C. It is interesting that, logically, thin form III crystals did not develop from the originally thick lamellae, and therefore peak III was not detected.

FTIR data on heating and cooling processes: Hydrogen bonds and methylene arrangements

FTIR is a powerful technique to obtain information about hydrogen bond interactions and the arrangement of methylene sequences in aliphatic polyamides [45,46]. Thus, the wavenumber of the Amide A band (NH stretching mode) is directly related to the strength of intermolecular hydrogen bonds. Figure 9 shows how this band shifts to higher frequencies with increasing temperature and to lower ones with decreasing it. Spectra of samples recorded at room temperature also show clear differences depending on the way they were processed. The maximum and minimum wavenumber values were found for the as-synthesized and melt crystallized samples, respectively. This, together with the X-ray diffraction data, clearly points out that hydrogen bonds were weaker for form I and stronger for form II, with the wavelength being dependent on the ratio between these forms, as inferred from the intermediate value found in the spectrum of a melt quenched sample that had an increasing ratio of form I.

It is highly interesting to note that the temperature evolution of the wavelength changed significantly in the 70-120 °C range for both melt crystallized and quenched samples, suggesting a transition where hydrogen bonding geometry changed. The DSC traces also showed that these samples had a broad exotherm that could be interpreted as a structural change. In contrast, this exothermic peak was not detected in the heating run of the as synthesized sample. Likewise, the abrupt wavenumber change was not observed in the FTIR spectra, either. However, caution must be taken since the frequency of Amide I had a small variation due to its high initial value. WAXD data showed a continuous evolution from the two peak structure towards the pseudohexagonal form. Therefore, the absence of a defined transition from FTIR or DSC data seems logical. Interpretation of the melt crystallized sample (and even the

melt quenched sample) is more confusing but the obtained spectra point out that form II and the pseudohexagonal form resulting from the Brill transition are clearly different, with hydrogen bonds being stronger for the former if the effect of unit cell expansion is not considered.

Structural changes involving amide groups can also be detected from the evolution of the amide II band (coupling of C-N stretching mode with N-H in plane bending mode), as displayed in Figure 10a. A broad band observed at 1534 cm^{-1} in the FTIR spectrum of an as-synthesized sample at room temperature (form I) moved slightly to 1540 cm^{-1} in the predominant form II obtained after slow crystallization from the maximum temperature allowed by the equipment (i.e., $200\text{ }^{\circ}\text{C}$). During the heating process, the FTIR spectrum changed drastically because of the progressive transformation of form I into form III and also of unit cell expansion. Furthermore, new narrow bands at 1557 , 1524 and 1508 cm^{-1} appeared together with the above band at 1541 cm^{-1} as a result of the complex hydrogen bonding arrangement attained at high temperature.

Although the amide III region is also sensitive to secondary structural changes, its potential has not been extensively explored due to its complexity since it results from a combination of C-N stretching and N-H bending modes. However, Figure 11b shows clear differences between spectra that reflect the wavenumber dependence on the crystalline form. Specifically, a band at 1286 cm^{-1} could be associated with form I since it could be seen in the spectrum of the as-synthesized sample and diminished when this form was minority. Interestingly, this band was slightly more intense in the spectrum of the quenched sample than in the melt crystallized one, suggesting again a greater ratio of form I when the sample was obtained by rapid cooling from the melt.

The Amide V band (out of plane C-H bending) was also dependent on the crystalline structure, as shown in Figure 11c for some representative spectra. Basically, this band

appeared at 680 cm^{-1} in the spectrum of form I taken at room temperature whereas a second band was observed at 671 cm^{-1} in room temperature spectra of samples having a predominant form II. The slight shift towards lower frequency of Amide V is difficult to interpret since it is also influenced by the occurrence of twisting around the $\text{CH}_2\text{-NH}$ bonds.

Great changes were also detected in bands in the 1480 to 1410 cm^{-1} region (Figure 10b), which were associated with the CH_2 scissoring mode. Specifically, the intensity of the band at 1458 cm^{-1} gradually increased with temperature, and could therefore be associated with form III. Room temperature spectra of as-synthesized and melt crystallized samples showed distinctive bands, like those at 1475 and 1417 cm^{-1} , which were found in the spectra of samples having a predominant form I structure. Obviously, these structural changes also involved methylene groups with increased motion at high temperatures.

Figure 11a shows bands associated with vibrational modes of methylene groups (e.g., C-C skeletal backbone for the $1210\text{-}1120\text{ cm}^{-1}$ region) that depend on the crystalline structure. Thus, bands at 1152 cm^{-1} and 1199 cm^{-1} can be associated with forms II and I, respectively. It could also be observed that the second band was more intense in the spectrum of the quenched sample than of the melt crystallized sample, in full agreement with the above observations on amide I and amide III bands.

Spherulitic morphologies: Changes induced by temperature

Previous data on melt crystallized nylon 6 9 samples were rather confusing since different spherulitic morphologies were reported and even both, positive and negative spherulites were found at a common crystallization temperature (i.e., $230\text{ }^\circ\text{C}$) [39]. Mixed spherulites that combined areas of low positive birefringence and higher negative

birefringence were also described for crystallizations in the 215-230 °C interval. In fact, 219 °C was determined as the temperature at which low birefringence spherulites were formed, and indeed changes in the birefringence sign (negative or positive) could occur by increasing or decreasing the temperature, respectively. Finally, ringed spherulites with a zig-zag extinction pattern were described for crystallization temperatures below 190 °C. The behavior of other even-odd nylons was also rather complex. For example, a similar reversible change in the optical sign was described for low birefringence spherulites of nylon 4 9 around a temperature of 236 °C when samples were slowly (1 °C/min) cooled (negative sign) or heated (positive sign) [39]. Interestingly, no changes were observed when cooling/heating rates were high (e.g., 20 °C/min).

Some points remain unclear and need to be evaluated using the above X-ray, DSC and FTIR data. Specifically, the observed reversibility of the birefringence sign is peculiar and obviously cannot be observed in conventional even-even nylons where a single hydrogen bonding direction exists. This direction corresponds to that of the maximum refractive index and may be oriented along a radial (positive birefringence) or a tangential (negative birefringence) spherulite direction [38,47]. Therefore, a change on the birefringence sign of even-even polyamides should imply a different spatial disposition of constitutive lamellae. Specifically, a rotation of 90° around an axis parallel to the molecular chain axis (i.e., tangential to the spherulite) is required. Note that this rotation is completely different from the well-known lamellar twisting which implies rotation along spherulite radial directions. In any case, a lamellar reorientation cannot occur once the spherulite is formed and consequently temperature induced reversible changes on the birefringence sign are unexpected. In other words, it seems highly unlikely that hydrogen bonds changed from radial to tangential direction by a simple variation of temperature.

The direction of maximum refractive index is more difficult to determine when hydrogen bonds are established along two directions instead of the single direction found in even-even polyamides. Therefore, it may be interesting to address the peculiarities observed for even-odd nylons considering their unusual hydrogen bonding arrangements and the observed polymorphism since small changes between the two hydrogen bonding directions may modify the resulting optical properties.

Figure 12 is an optical micrograph of a single spherulite isothermally stepwise crystallized at different decreasing temperatures that corresponded to the limits (232, 225, 220 and 215 °C) at which the different morphologies developed. As can be seen, great morphological changes occur in a very narrow temperature interval, leading to confusing results. X-ray diffraction data indicated that nylon 69 always crystallized in form III at the test temperatures, and consequently differences in optical properties cannot be justified assuming different crystalline structures.

Figure 13 shows the characteristic spherulites obtained in a fully reproducible way for each selected temperature. Crystallization was very slow at temperatures higher than 232 °C, giving rise to large spherulites (diameters between 300 and 500 μm) with a positive birefringence and composed of slender edge-on crystalline lamellae with apparent preference for growth in the axial direction (i.e., axialites) also clearly detected in AFM micrographs (Figure 14a). The observed positive birefringence is opposite to that found in even-even nylons crystallized at temperatures close to their melting point and may reflect the different Brill structure between the two families of nylons (e.g., a single hydrogen bonding direction or multiple hydrogen bonding directions for the even-even and even-odd series, respectively).

The appearance and optical properties of spherulites changed drastically around 225 °C. In fact, a very low, poor birefringence was observed (especially in black and white

micrographs taken without the first-order red tint plate, see inset of Figure 12). However, a predominant positive sign was observed at this temperature. The low birefringence suggests a morphology consisting of flat-on crystals which have a lower anisotropy than edge-on lamellae. These crystals can be observed even in AFM micrographs (Figure 14b). Thus, the change of optical properties (i.e., high and low birefringence) can be easily explained in terms of edge-on or flat-on disposition of lamellae achieved by a rotation along the spherulite radial direction.

Typical ringed spherulites with a negative birefringence and ring spacing within a 5-7 μm range were observed between 225 °C and 215 °C (Figure 13c). Thus, lamellar twisting was characteristic of this temperature interval. The structure defined by different hydrogen bonding directions might have led to a different birefringence sign according to the tilting angle since it is a more complex system than that defined by a single direction where only radial or tangential dispositions can be considered for non-planar lamellae. Finally, typical fibrillar morphologies with a well-defined Maltese cross and positive birefringence were characteristic of crystallizations performed at temperatures lower than 215 °C (Figure 13d). Note that the birefringence sign was similar to that observed for axialites found at the highest temperature. A peculiar birefringence was only detected for ringed spherulites (i.e., those with a clear lamellar twisting).

Figure 15 shows polarized optical micrographs of a nylon 6 9 spherulite isothermally crystallized at 225 °C and taken at this temperature and at room temperature after cooling as well as at 80 °C and 128 °C during a subsequent heating process. It is clear that the birefringence sign is completely dependent on temperature. Moreover, a significant change was found in samples observed at the crystallization temperature (positive birefringence) and after the cooling process (negative birefringence). White

and yellow dashed circles point out crystalline domains that initially had positive and negative birefringence, respectively. The change in the optical sign clearly suggests a structural transition that influenced the optical properties significantly when lamellae had a flat-on lamellar disposition. According to X-ray diffraction data, form III was found at high temperature whereas form II was predominant at room temperature. Note that small changes in the angle between the two hydrogen bonding directions may influence the birefringence sign, especially when it was initially low. Reversibility of the optical sign was detected when samples were slowly reheated (1 °C/min), as expected from the achievement of form III. Figures 15c and 15d demonstrate that the birefringence change occurred at temperatures higher than 80 °C and ended around 128 °C since no modifications were observed at higher temperatures. The main point is that X-ray diffraction data indicated that structural transitions (e.g., from form III to forms II or I) occurred precisely in the above temperature range, supporting the interpretation of reversibility in terms of different polymorphic forms based on the arrangements with two hydrogen bonding directions.

CONCLUSIONS

In summary, WAXD, FTIR and DSC data pointed out a complex structural behaviour of nylon 6 9 during heating and cooling processes that contrast with that reported for conventional even-even polyamides. The peculiar structure of nylon 6 9 makes feasible the easy occurrence of polymorphic transitions, which are based on slight changes in the angle between the two hydrogen bonding directions. More interestingly, structural transitions may justify a temperature induced reversible change of the sign of optical birefringence when spherulites have a flat-on lamellar disposition. In any case, the

present work points out a system with unusual optical properties that can be rationalized in terms of crystalline structure and morphology.

Acknowledgments

Authors are in debt to supports from MINECO and FEDER (MAT2012-36205) and the Generalitat de Catalunya (2014SGR188). S.K.M. acknowledges an FPI grant from MINECO. Diffraction experiments were performed at NCD beamline at ALBA Synchrotron with the collaboration of ALBA staff.

REFERENCES

- [1] van Veltoen JLJ, Gootjes L, Noordover BAJ, Meuldijk J. Bio-based, amorphous polyamides with tunable properties. *Eur. Polym. J.* 2015;66:57-66. doi:10.1016/j.eurpolymj.2015.01.040.
- [2] Jasinska L, Villani M, Wu J, van Es DS, Klop E, Rastogi S. Novel, fully biobased semicrystalline polyamides. *Macromolecules* 2011;44:3458-66. doi:10.1021/ma200256v.
- [3] Eltahir YA, Saeed HAM, Haroon AM, Chen YJ, Xia YM, Wang YM. Effect of hot drawing on the structure and properties of novel polyamide 5,6 fibers. *Text. Res. J.* 2014;84:1700-7. doi: 10.1177/0040517514527378.
- [4] Eltahir YA, Saeed HAM, Yuejun C, Xia Y, Yimin W. Parameters characterizing the kinetics of the non-isothermal crystallization of polyamide 5,6 determined by differential scanning calorimetry. *J. Polym. Eng.* 2014;34:353-8. doi: 10.515/polymeng-2013-0250.
- [5] Jiang JD, Zhang K, Liu CY, Wu GZ. Thermal expansion behavior of aliphatic polyamides. *Acta Polym. Sin.* 2013;2:255-62. doi: 10.3724/SP.J.1105.2013.12241.
- [6] Li YL, Hao XM, Guo YF, Chen X, Yang Y, Wang JM. Study on the acid resistant properties of bio-based nylon 56 fiber compared with the fiber of nylon 6 and nylon 66. *Adv. Mater. Res.* 2014;1048:57-61. doi: 10.4028/www.scientific.net/AMR.1048.57.
- [7] Capsal JF, Dantras E, Dandurand J, Lacabanne C. Dielectric relaxations and ferroelectric behavior of even-odd polyamide PA6,9. *Polymer* 2010;51:4606-10. doi: 10.1016/j.polymer.2010.07.040.
- [8] Samanta S, He J, Selvakumar S, Lattimer J, Ulven C, Sibi M, Bahr J, Chisholm BJ. Polyamides based on the renewable monomer, 1,13-tridecanediamine II: Synthesis and

characterization of nylon 13,6. *Polymer* 2013;54:1141-9. doi: 10.1016/j.polymer.2012.12.034.

[9] Liu S, Cui Z, Fu P, Liu M, Zhang L, Li Z, Zhao Q. Ferroelectric behavior and polarization mechanism in odd-odd polyamide 11,11. *J Polym. Sci. Part B: Polym. Phys* 2014;52:1094-9. doi: 10.1002/polb.23537.

[10] Scheinbeim JI, Lee JW, Newman BA. Ferroelectric Polarization Mechanisms in Nylon 11. *Macromolecules* 1992;25:3729-32. doi: 10.1021/ma000409019.

[11] Bunn CW, Garner E V. The crystal structures of two polyamides ('Nylons'). *Proc R Soc A Math Phys Eng Sci* 1947;189:39–68. doi:10.1098/rspa.1947.0028.

[12] Xenopoulos A, Clark ES. Nylon Plastics Handbook. In: Kohan MI, editor. *Nylon Plast. Handb.* 4th ed., Munich: Hanser Publishers; 1995, p. 108.

[13] Kinoshita Y. An investigation of the structures of polyamide series. *Die Makromol Chemie* 1959;33:1–20. doi:10.1002/macp.1959.020330101.

[14] Bella J, Puiggali J, Subirana JA. Glycine residues induce a helical structure in polyamides. *Polymer* 1994;35:1291–7. doi:10.1016/0032-3861(94)90026-4.

[15] Puiggali J, Aceituno JE, Navarro E, Campos JL, Subirana JA. Structure of n,3 Polyamides, a Group of Nylons with Two Spatial Hydrogen-Bond Orientations. *Macromolecules* 1996;29:8170–9. doi:10.1021/ma960069k.

[16] Navarro E, Franco L, Subirana JA, Puiggali J. Nylon 65 has a unique structure with two directions of hydrogen bonds. *Macromolecules* 1995;28:8742–50. doi:10.1021/ma00130a006.

[17] Morales-Gómez L, Ricart A, Franco L, Puiggali J. Study on the Brill transition and melt crystallization of nylon 65: A polymer able to adopt a structure with two hydrogen-bonding directions. *Eur Polym J* 2010;46:2063–77. doi:10.1016/j.eurpolymj.2010.07.010.

- [18] Navarro E, Subirana JA, Puiggali J. The structure of nylon 12,5 is characterized by two hydrogen bond directions as are other polyamides derived from glutaric acid. *Polymer* 1997;38:3429–32. doi:10.1016/S0032-3861(97)00017-7.
- [19] Morales-Gómez L, Casas MT, Franco L, Puiggali J. Structural transitions of nylon 47 and clay influence on its crystallization behavior. *Eur Polym J* 2013;49:1354–64. doi:10.1016/j.eurpolymj.2013.02.030.
- [20] Franco L, Cooper SJ, Atkins EDT, Hill MJ, Jones NA. Nylon 6 9 can crystallize with hydrogen bonding in two and in three interchain directions. *J Polym Sci Part B Polym Phys* 1998;36:1153–65. doi:10.1002/(SICI)1099-0488(199805)36:7<1153::AID-POLB6>3.0.CO;2-V.
- [21] Puiggali J, Franco L, Alemán C, Subirana JA. Crystal structures of nylon 5,6. A model with two hydrogen bond directions for nylons derived from odd diamines. *Macromolecules* 1998;31:8540–8. doi:10.1021/ma971895b.
- [22] Morales-Gómez L, Soto D, Franco L, Puiggali J. Brill transition and melt crystallization of nylon 56: An odd–even polyamide with two hydrogen-bonding directions. *Polymer* 2010;51:5788–98. doi:10.1016/j.polymer.2010.09.074.
- [23] Villaseñor P, Franco L, Subirana JA, Puiggali J. On the crystal structure of odd-even nylons: Polymorphism of nylon 5,10. *J Polym Sci Part B Polym Phys* 1999;37:2383–95. doi:10.1002/(SICI)1099-0488(19990901)37:17<2383::AID-POLB9>3.0.CO;2-G.
- [24] Franco L, Subirana JA, Puiggali J. Structure and morphology of odd polyoxamides [Nylon 9,2]. A new example of hydrogen-bonding interactions in two different directions. *Macromolecules* 1998;31:3912–24. doi:10.1021/ma971599z.

- [25] Nakagawa T, Nozaki K, Maeda S, Yamamoto T. Polymorphism of poly(nonamethyleneoxamide) crystal. *Polymer* 2015;57:99-104. doi: 10.1016/j.polymer.2012.12.022.
- [26] Cui X, Yan D. Preparation, characterization and crystalline transitions of odd-even polyamides 11, 12 and 11,10. *Eur. Polym. J.* 2005;41:863-70. doi: 10.1016/j.eurpolymj.2004.10.045.
- [27] Nakagawa T, Maeda S, Nazaki K, Yamamoto T. Crystal structure of an aliphatic polyoxamide containing methyl side-groups: Poly(2-methyl-1,8-octamethyleneoxamide). *Polymer* 2014;55:2254-61. doi: 101016/j.polymer2014.03.009.
- [28] Brill R. Beziehungen zwischen wasserstoffbindung und einigen eigenschaften von polyamiden. *Die Makromol Chemie* 1956;18:294–309. doi:10.1002/macp.1956.020180125.
- [29] Wendoloski JJ, Gardner KH, Hirschinger J, Miura H, English AD. Molecular dynamics in ordered structures: computer simulation and experimental results for nylon 66 crystals. *Science* 1990;247:431–6. doi:10.1126/science.247.4941.431.
- [30] Feldman AY, Wachtel E, Vaughan GBM, Weinberg A, Marom G. The Brill Transition in Transcrystalline Nylon-66. *Macromolecules* 2006;39:4455–9. doi:10.1021/ma060487h.
- [31] Nair SS, Ramesh C, Tashiro K. Crystalline phases in nylon-11: Studies using HTWAXS and HTFTIR. *Macromolecules* 2006;39:2841-2848. doi: 10.1021/ma052597e.
- [32] Wolanov Y, Feldman AY, Harel H, Marom G. Amorphous and crystalline phase interaction during the Brill transition in nylon 66. *Express Polym. Lett.* 2009;3:452-7. doi: 10.3144/espresspolymlett.2009.55.

- [33] Wang C, Tsou SY, Lin HS. Brill transition of nylon-6 in electrospun fibers. *Colloid Polym. Sci.* 2012;290:1799-1809. doi: 10.1007/500396-012-2724-9.
- [34] Suzuki H, Ishii S, Sato H, Yamamoto S, Morisawa Y, Ozaki Y, et al. Brill transition of nylon-6 characterized by low-frequency vibration through terahertz absorption spectroscopy. *Chem Phys Lett* 2013;575:36–9. doi:10.1016/j.cplett.2013.05.002.
- [35] Yoshioka Y, Tashiro K. Structural change in the Brill transition of Nylon m/n (1) Nylon 10/10 and its model compounds. *Polymer* 2003;44:7007–19. doi:10.1016/j.polymer.2003.04.001.
- [36] Yoshioka Y, Tashiro K. Structural Changes in Phase Transitions of Nylon Model Compounds. 1. Transition Behavior of Model Compounds of R-NHCO-R' Type. *J Phys Chem B* 2003;107:11835–42. doi:10.1021/jp0224160.
- [37] Tashiro K, Yoshioka Y. Conformational disorder in the Brill transition of uniaxially-oriented nylon 10/10 sample investigated through the temperature-dependent measurement of X-ray fiber diagram. *Polymer* 2004;45:6349–55. doi:10.1016/j.polymer.2004.07.024.
- [38] Lovinger AJ. Crystallographic factors affecting the structure of polymeric spherulites. I. Morphology of directionally solidified polyamides. *J Appl Phys* 1978;49:5003. doi:10.1063/1.324447.
- [39] Magill JH. Formation of spherulities in polyamides. IV. Even–odd polyamides and poly(ω -aminocarboxylic acids). *J Polym Sci Part A-2 Polym Phys* 1969;7:123–42. doi:10.1002/pol.1969.160070110.

- [40] Lugito G, Woo EM, Lamellar assembly corresponding to transitions of positively to negatively birefringent spherulites in poly(ethylene adipate) with phenoxy. *Colloid Polym. Sci.* 2013;291:817-26. doi: 10.1007/500396-012-2793-9.
- [41] Woo EM, Chou YH, Chiang WJ, Chen IT, Huang IH, Kuo NT. Amorphous phase behavior and crystalline morphology in blends of poly(vinyl methyl ether) with isomeric polyesters: poly(hexamethylene adipate) and poly(ϵ -caprolactone). *Polym. J.* 2010;42:391-400. doi: 10.1038/PJ.2010.18.
- [42] Hsieh YT, Woo EM. Microscopic Lamellar Assembly and Birefringence Patterns in Poly(1,6-hexamethylene adipate) Packed with or without Amorphous Poly(vinyl methyl ether). *Ind. Eng. Chem. Res.* 2013;52:3779-86. doi: 10.1021/ie303221C.
- [43] Lugito G, Yang CY, Woo EM. Phase-separation induced lamellar re-assembly and spherulite optical birefringence reversion. *Macromolecules* 2014;47:5624-32. doi: 10.1021/ma5011556.
- [44] Hoffman JD, Weeks JJ. Melting process and the equilibrium melting temperature of polychlorotrifluoroethylene. *J Res Natl Bur Stand Sect A Phys Chem* 1962;66A:13. doi:10.6028/jres.066A.003.
- [45] Cooper SJ, Coogan M, Everall N, Priestnall I. A polarised μ -FTIR study on a model system for nylon 6 6: implications for the nylon Brill structure. *Polymer* 2001;42:10119–32. doi:10.1016/S0032-3861(01)00566-3.
- [46] Yoshioka Y, Tashiro K, Ramesh C. New interpretation of progression bands observed in infrared spectra of nylon-m/n. *J Polym Sci Part B Polym Phys* 2003;41:1294–307. doi:10.1002/polb.10457.
- [47] Lee SS, Phillips PJ. Melt crystallized polyamide 6.6 and its copolymers, Part II. Crystallization mechanisms in the homopolymer. *Eur Polym J* 2007;43:1952–62. doi:10.1016/j.eurpolymj.2007.01.056.

FIGURE CAPTIONS

Figure 1. a) Scheme of the unfavorable hydrogen bonding geometry between odd carboxamide (i.e., pimelamide) units having an all-trans conformation. b) Scheme showing the formation of hydrogen bonds along two directions when the two amide planes of the carboxamide unit rotate in opposite directions to the plane defined by its methylene carbon atoms. External chains (stick representation) should be shifted along the chain axis direction (see arrows) with respect to the central chain (ball and stick representation), thus giving rise to a monoclinic unit cell. Color code: nitrogen, blue; oxygen, red; carbon, gray; hydrogen, brown.

Figure 2. a) One-dimensional WAXD profiles of nylon 6 9 during heating (3 °C/min) from room temperature to a few degrees before fusion. Inset shows a three-dimensional representation of WAXD profiles of nylon 47 during heating (3 °C/min) from room temperature. Dashed white circles show the appearance and disappearance of characteristic peaks associated with different crystallographic forms at around 100 °C. b) One-dimensional WAXD profiles of nylon 6 9 during cooling (3 °C/min) from the melt state to room temperature. Green and red arrows indicate the appearance of form I and form II reflections, respectively. Dashed ellipsoid shows the temperature range where these two forms appeared. Blue lines indicate the evolution of weaker reflections of the form III.

Figure 3. a) Changes in intensity of the strongest reflection at 0.423-0.421 nm during cooling. b) Deconvolution of the X-ray diffraction profile of a sample non-isothermally crystallized from the melt showing characteristic spacings associated with the amorphous halo and forms I and II (the minor peak corresponding to residual form III was not considered).

Figure 4. a) One-dimensional WAXD profiles of nylon 6 9 taken at selected temperatures during heating and cooling scans (3 °C/min). Dashed lines represent the evolution of the main reflections. b) X-ray diffraction patterns taken at selected temperatures during the heating run to show the evolution of the two characteristic spacings of form I towards a single reflection associated with form III. No reflections associated with form II were detected.

Figure 5. DSC scans of the heating run of the as-synthesized sample (a), cooling run from the melt state (b), subsequent heating run (c) and heating run of a sample quenched from the melt state (d). Heating and cooling runs were performed at a rate of 20 and 10 °C/min, respectively. Inset of (d) shows a magnification of the region between the glass transition temperature and 250 °C, where an exothermic event could be detected.

Figure 6. DSC heating runs of as-synthesized nylon 6 9 samples performed up to 255 °C at the indicated heating rates.

Figure 7. DSC heating runs of nylon 6 9 samples crystallized from the melt at 232 °C (a), 228 °C (b), 225 °C (c), 220 °C (d), 218 °C (e) and 215 °C (f) and subsequently cooled to room temperature (at 20 °C/min).

Figure 8. Hoffman-Weeks plot of temperatures corresponding to the variable endothermic melting peak III versus crystallization temperature. Equilibrium melting temperature is explicitly indicated at the intersection point with the $T_m = T_c$ line.

Figure 9. a) Representation of the wavenumber of the Amide A absorption band during a heating run (3 °C/min) for as-synthesized, melt crystallized and melt quenched nylon 6

9 samples. b) Change in the Amide A absorption band during heating and cooling runs (3 °C/min) of the as-synthesized nylon 6 9 sample.

Figure 10. FTIR spectra showing the evolution of absorption bands in the 1585-1490 cm^{-1} (a) and 1485-1405 cm^{-1} (b) regions during heating from room temperature to 250 °C at a rate of 3 °C/min. In both cases, the spectrum taken at room temperature after cooling (3 °C/min) from 200 °C is provided at the top of each graph.

Figure 11. Representative FTIR spectra taken at room temperature showing the absorption bands in the 1225-1110 cm^{-1} (a), 1325-1235 cm^{-1} (b) and 700-660 cm^{-1} (c) regions for the as-synthesized (black), quenched (red) and melt crystallized (blue) samples. For the sake of completeness, spectra taken at 200 °C (form III, green) are also given.

Figure 12. Optical micrograph of a spherulite isothermally grown at the indicated consecutive decreasing temperatures. Inset shows a black and white micrograph to emphasize the low birefringence of the crystallization performed at 225 °C.

Figure 13. Optical micrographs taken at the respective crystallization temperature of nylon 6 9 spherulites obtained at 232 °C (a), 225 °C (b), 220 °C (c) and 215 °C (d).

Figure 14. Atomic force microscopy amplitude (left) and 3D height images (right) of a nylon 6 9 sample isothermally crystallized at 232 °C (a) and 225 °C (b) from the melt state.

Figure 15. Optical micrographs of nylon 6 9 spherulites grown at 225 °C and taken at the crystallization temperature (a), after cooling to 25 °C at 1 °C/min (b), after a subsequent heating to 80 °C at 1 °C/min (c) and after heating to 128 °C (d).

Representative zones with initial negative and positive birefringence that experienced temperature induced reversible changes are indicated by dashed squares and circles, respectively.

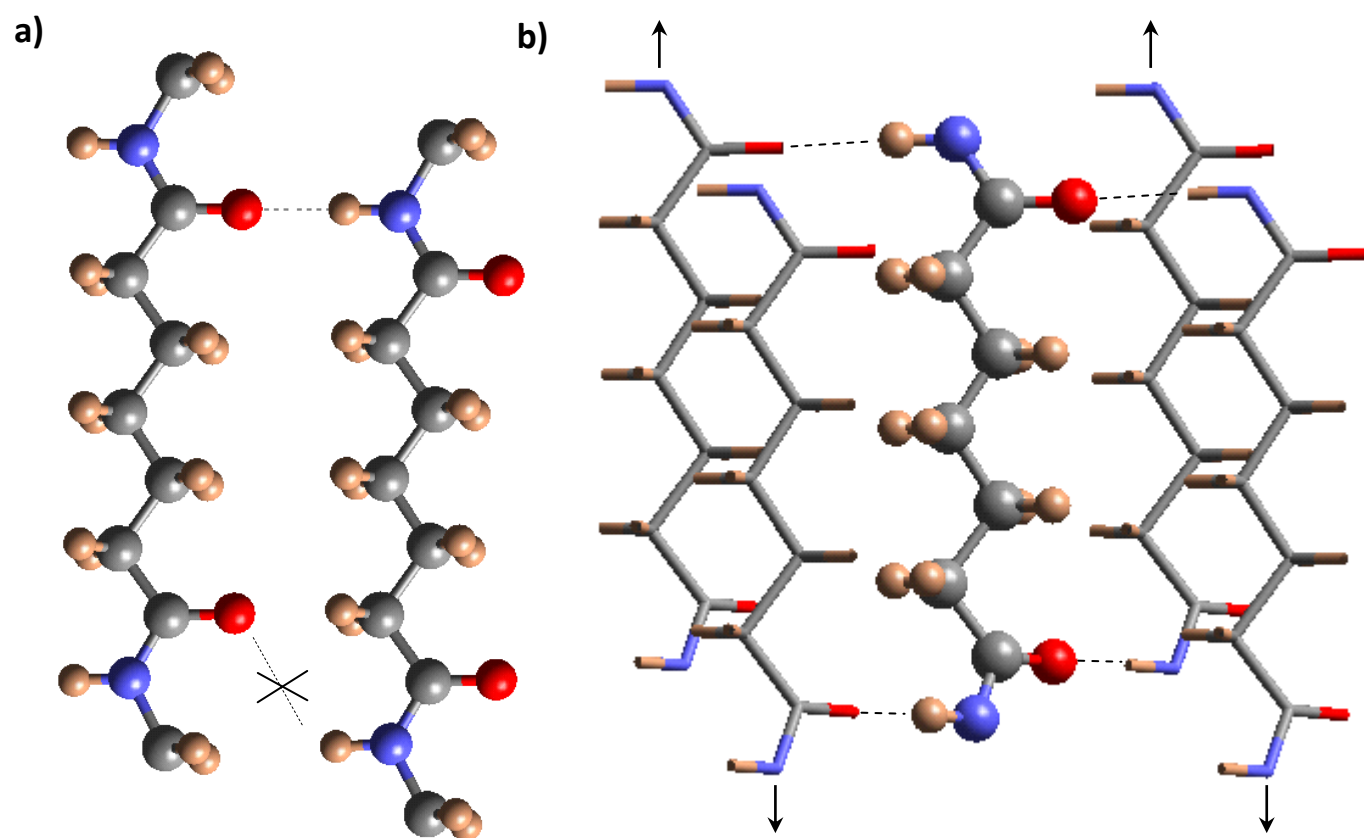


FIGURE 1
Murase et al.

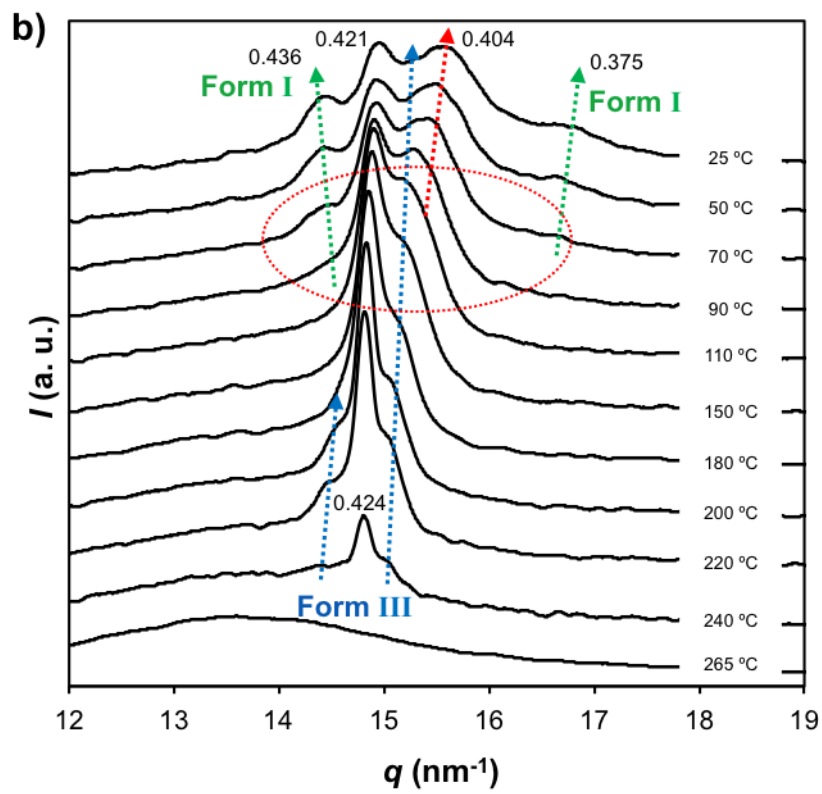
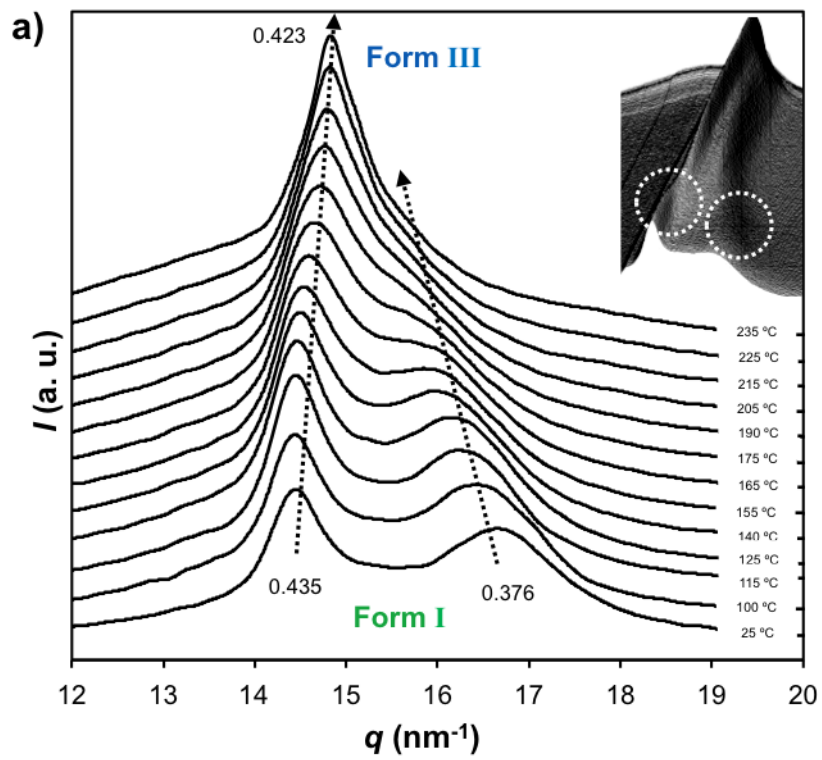


FIGURE 2
Murase et al.

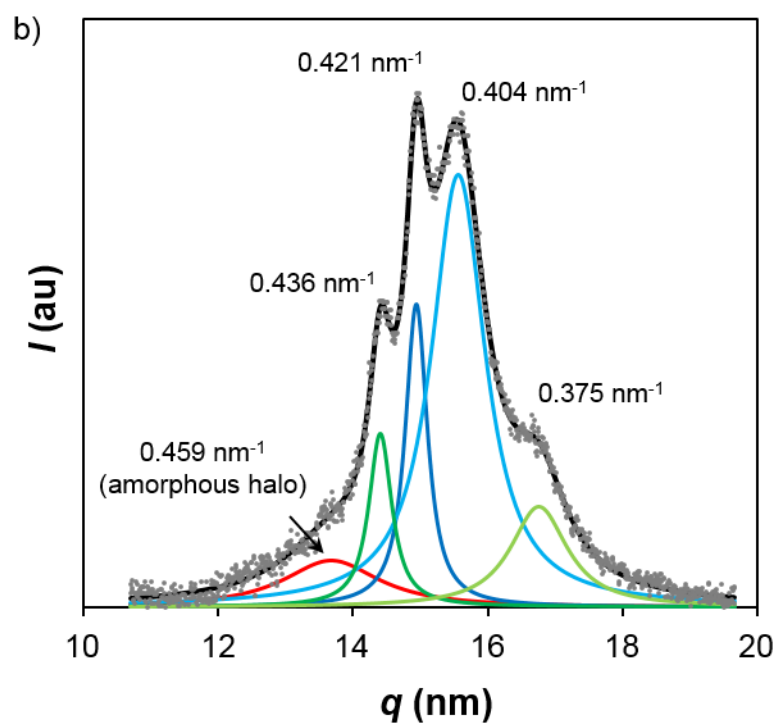
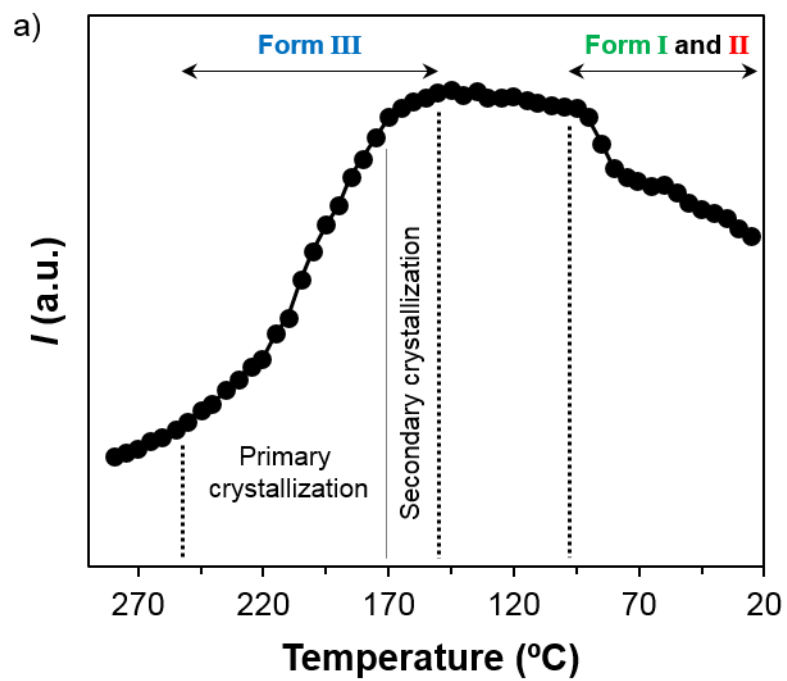


FIGURE 3
Murase *et al.*

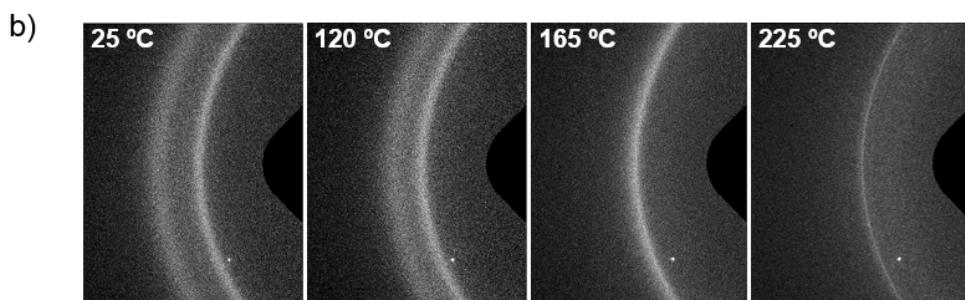
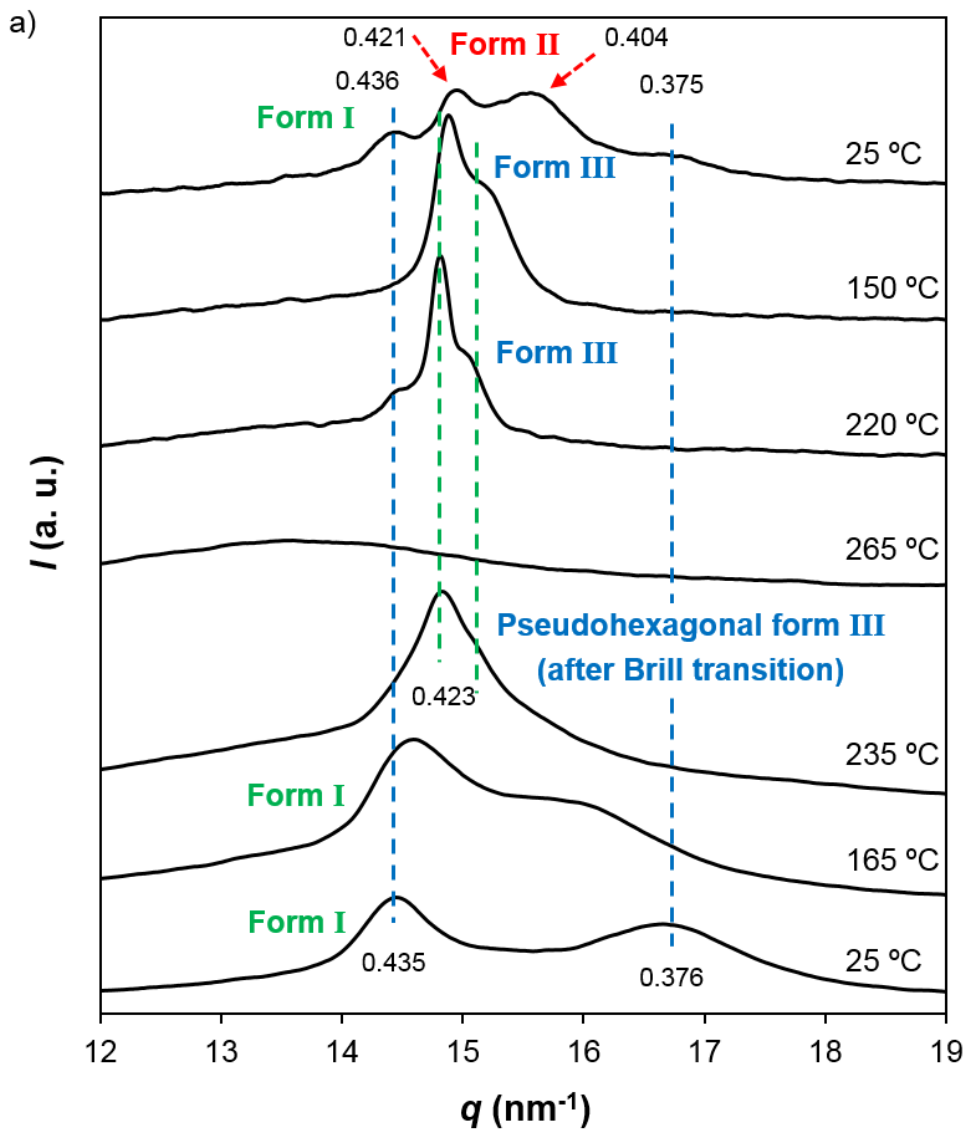


FIGURE 4
Murase et al.

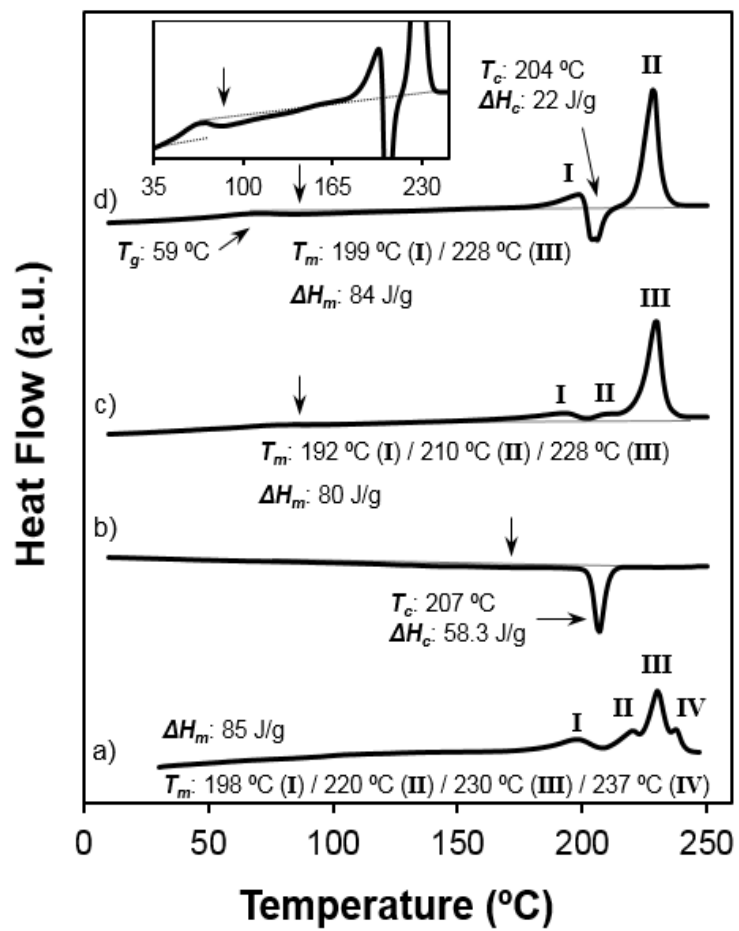


FIGURE 5
 Murase *et al.*

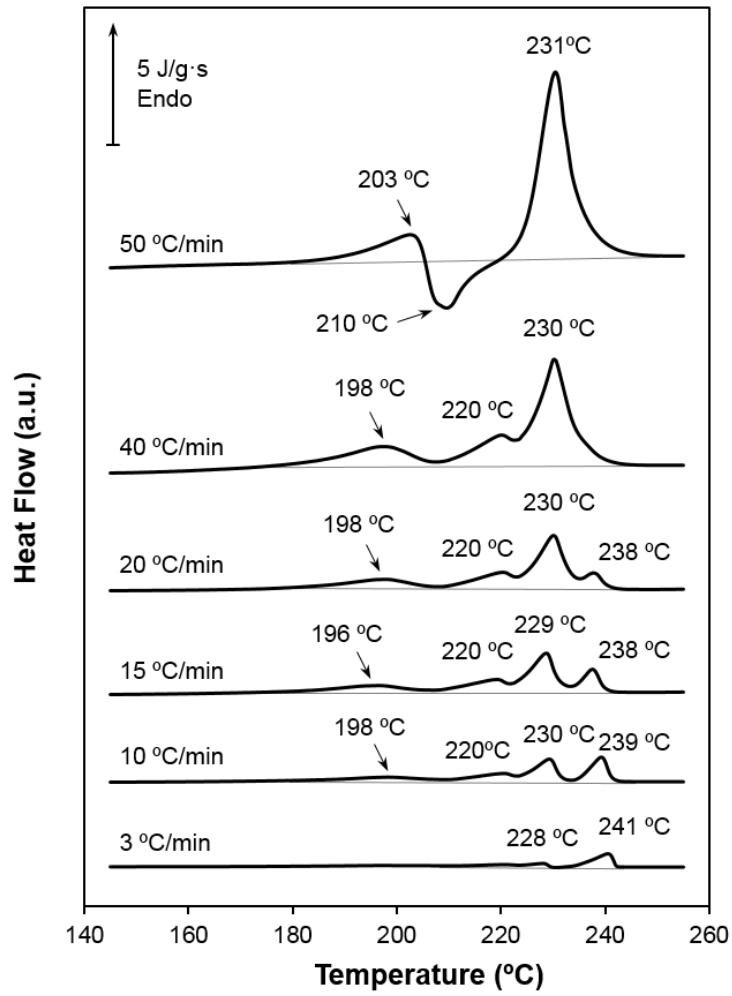


FIGURE 6
Murase *et al.*

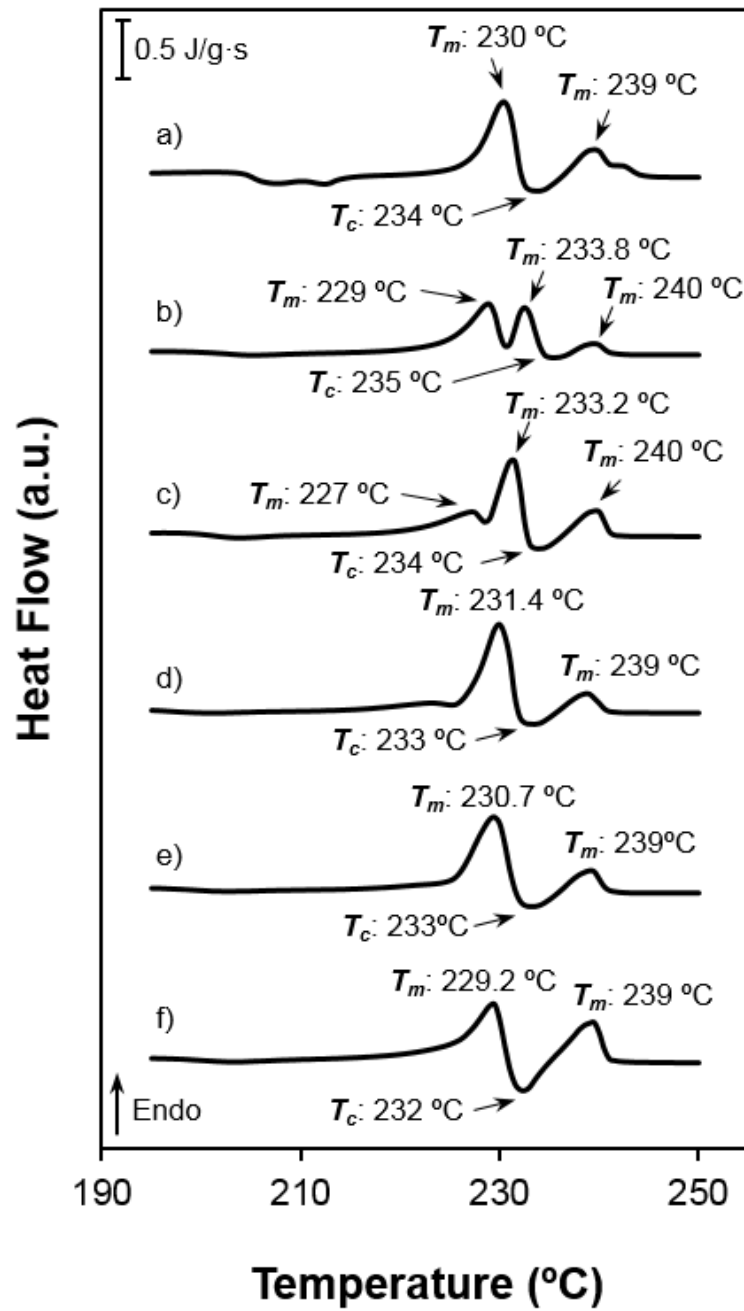


FIGURE 7
Murase *et al.*

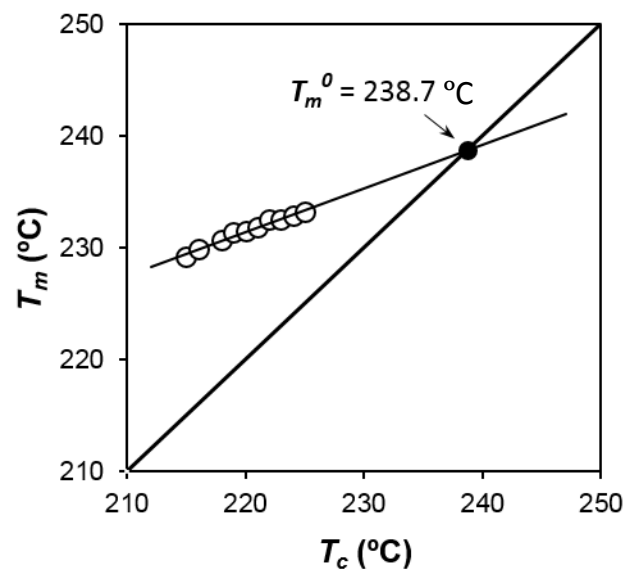


FIGURE 8
Murase et al.

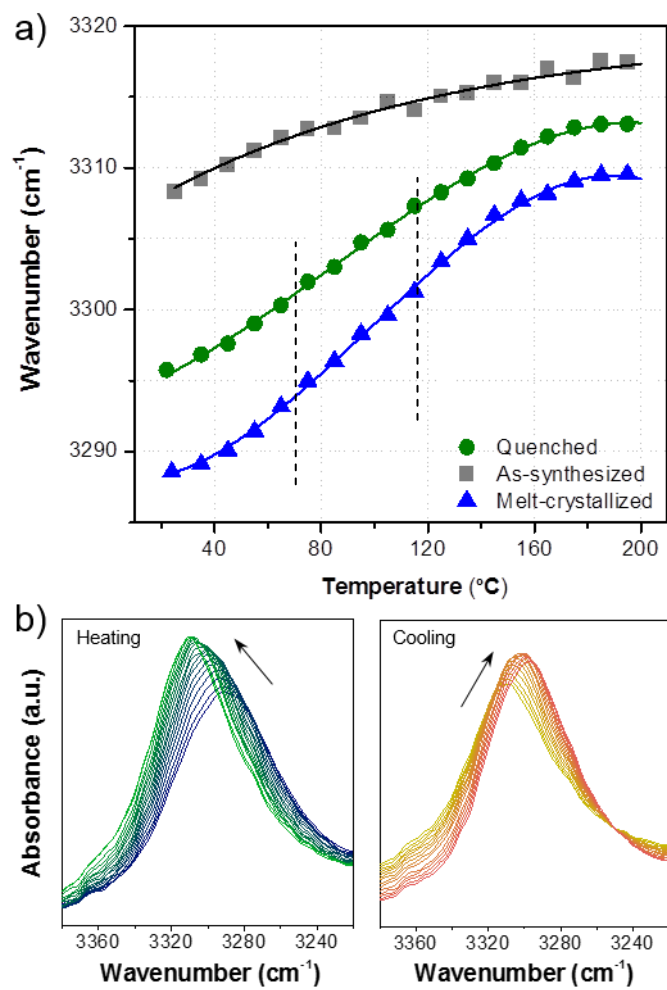


FIGURE 9
Murase et al.

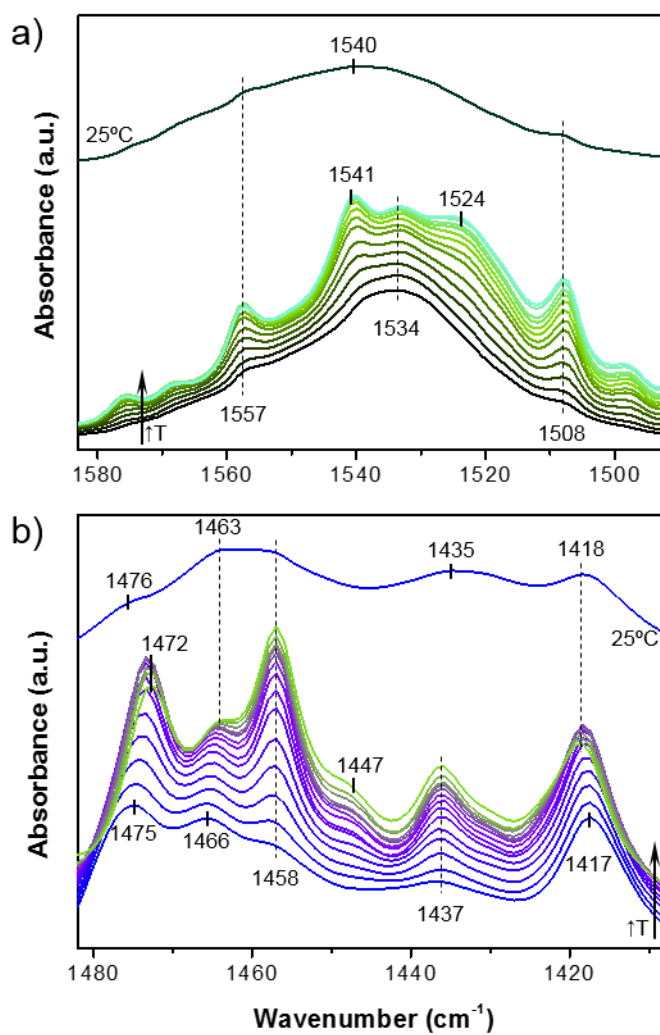


FIGURE10
Murase *et al.*

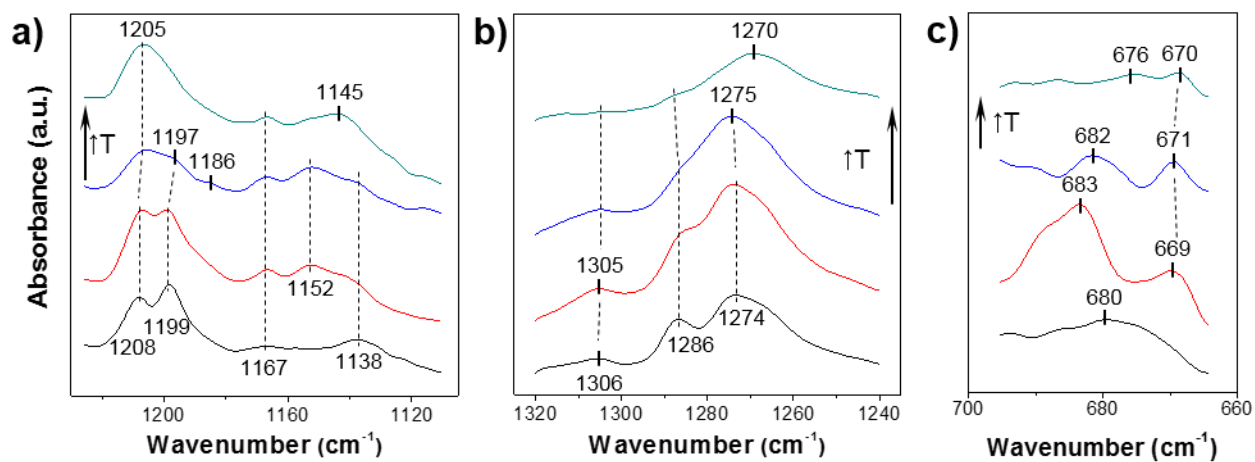


FIGURE 11
Murase *et al.*

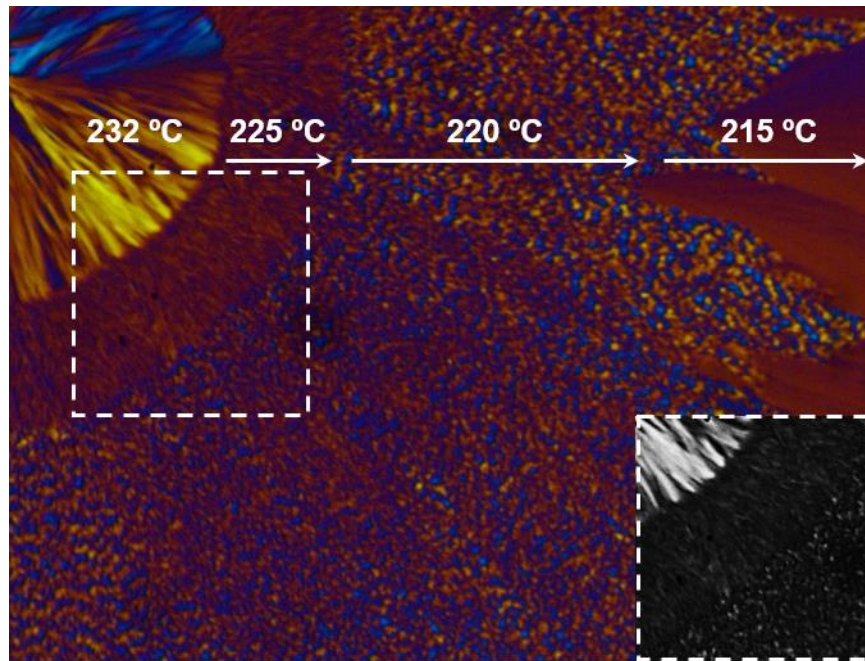


FIGURE 12
Murase *et al.*

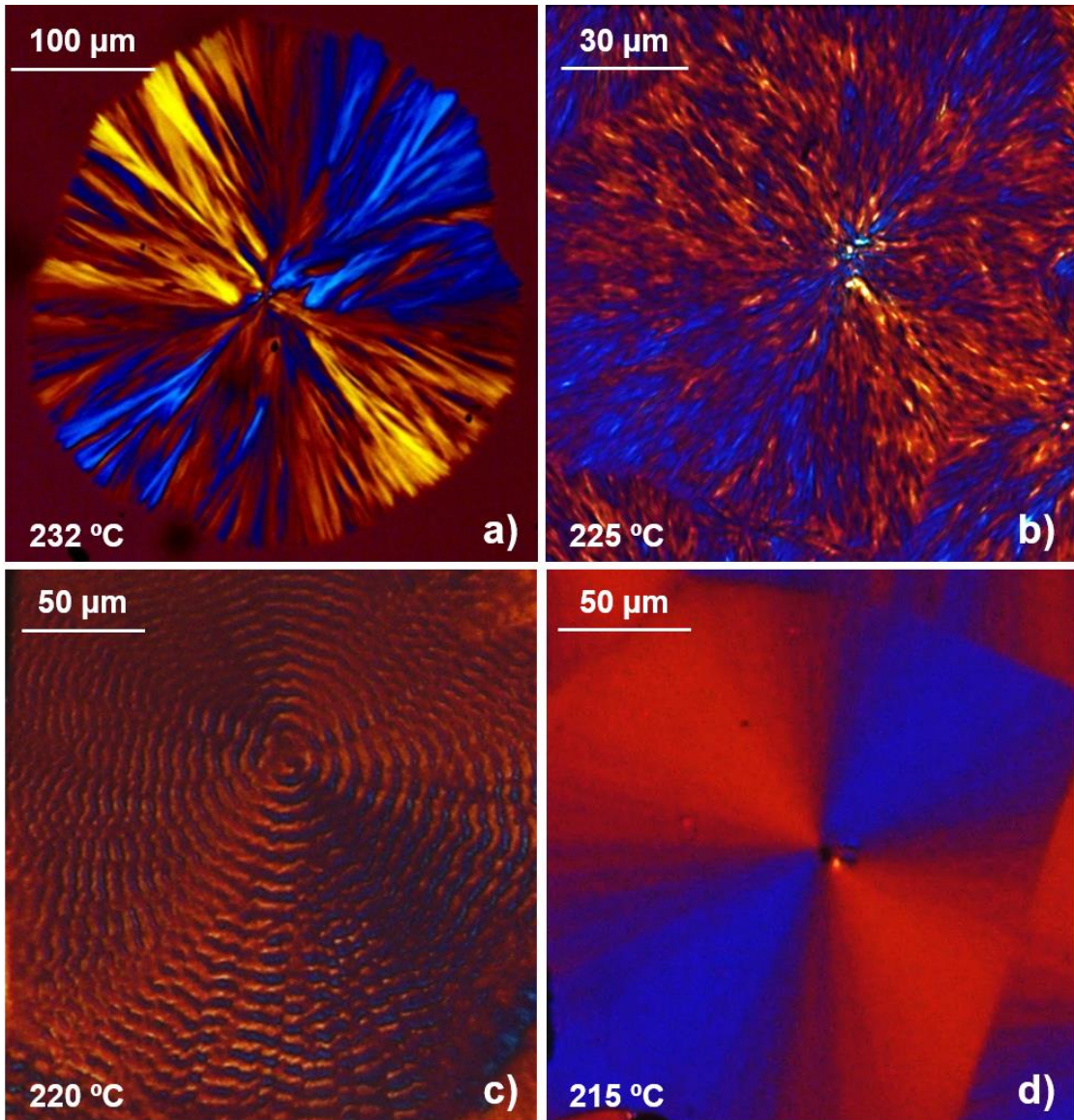


FIGURE 13
Murase et al.

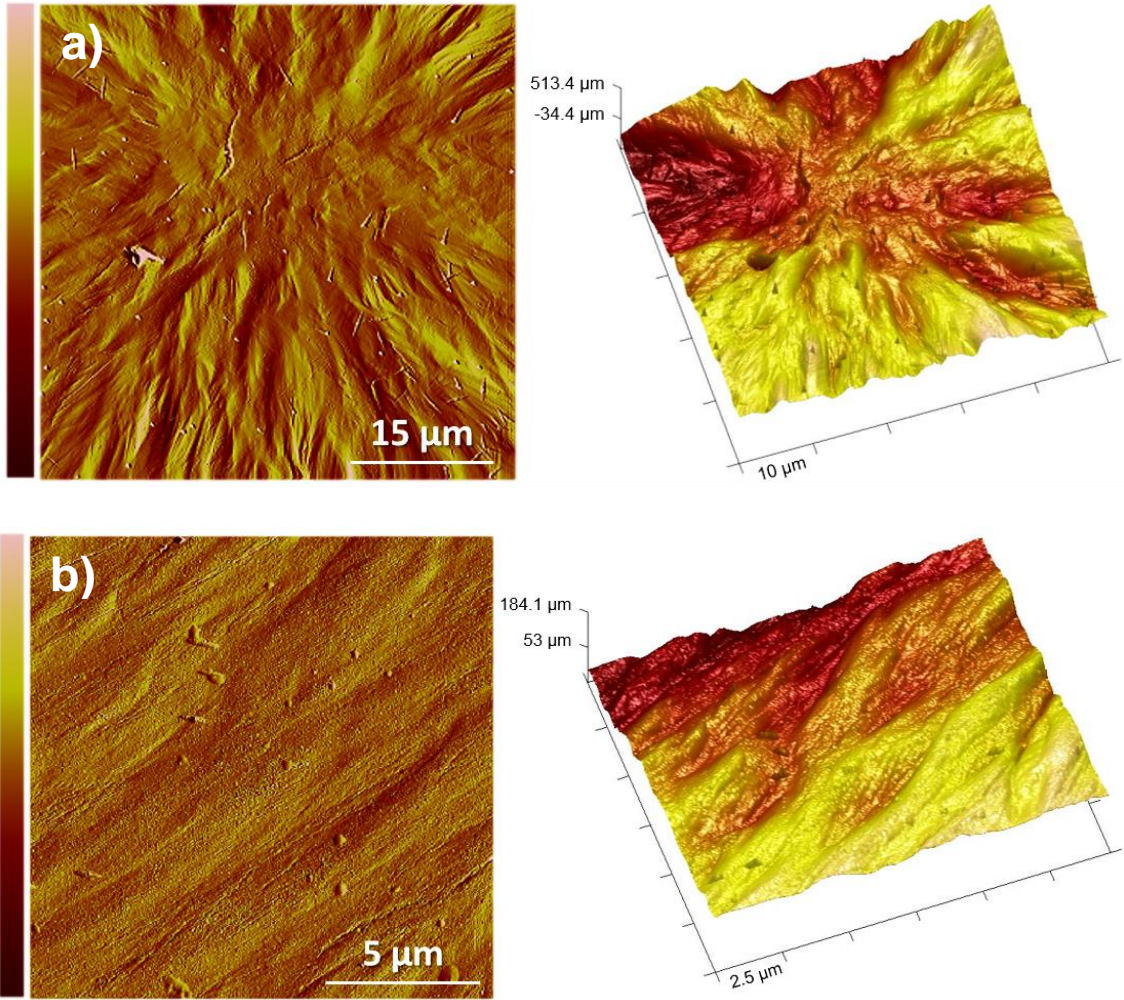


FIGURE 14
Murase *et al.*

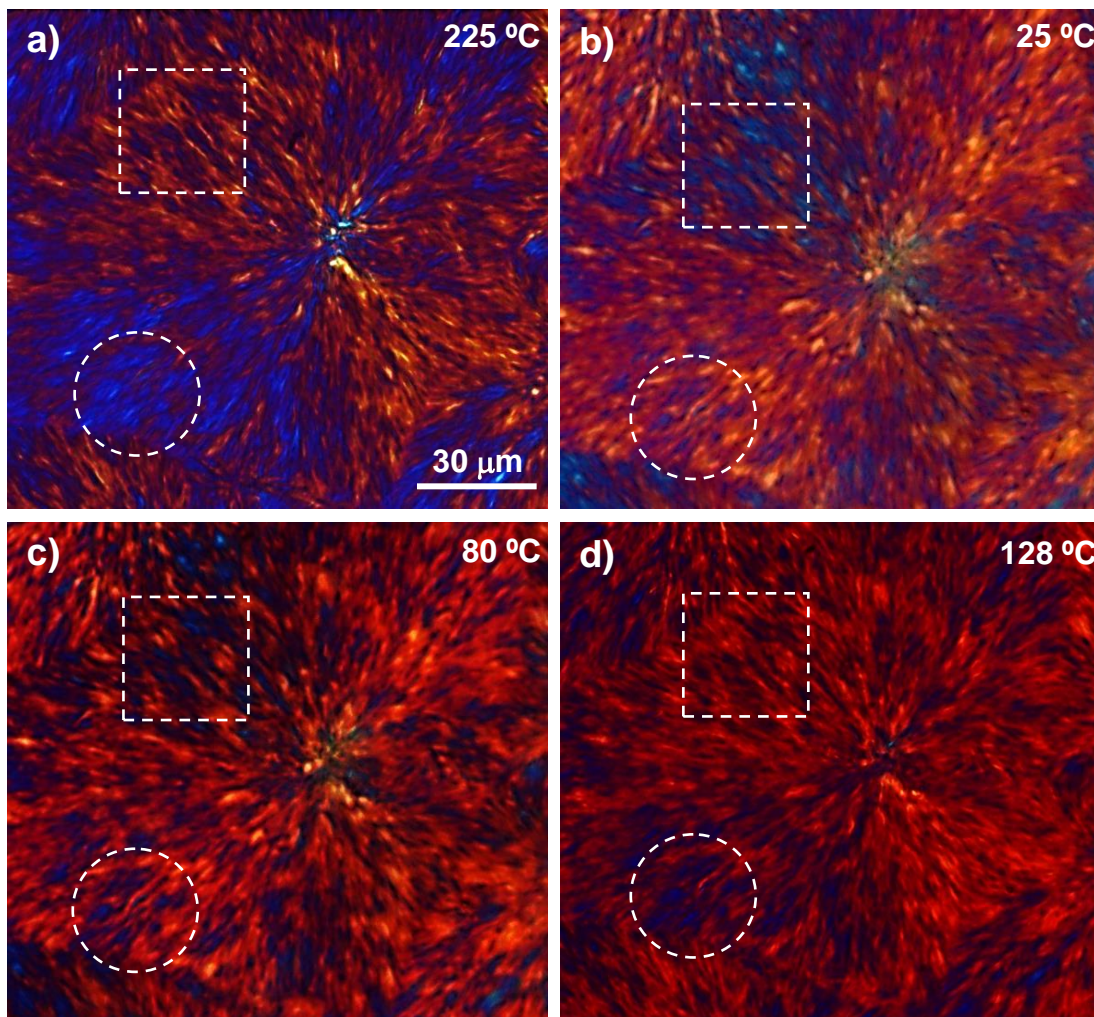


FIGURE 15
Murase et al.